Supporting Information

Core/Shell Microstructure Induced Synergistic Effect for Efficient Water-Droplet Formation and Cloud-Seeding Application

*Yanlong Tai[1], Haoran Liang[1], Nabil El Hadri[2], Ali M. Abshaev[3], Buzigit M. Huchinaev[3], Steve Griffith[1], Mustapha Jouiad[2], Linda Zou[1]**

[1]Department of Civil Infrastructure and Environment Engineering, Masdar Institute, Khalifa University of Science and Technology, Abu Dhabi, United Arab Emirates

[2]Department of Mechanical Engineering, Masdar Institute, Khalifa University of Science and Technology, Abu Dhabi, United Arab Emirates

[3]High Mountain Geophysical Institute of Russian Federal Hydrometeorological Service, Nalchik city, Kabardino-Balkarian, Republic, Russian Federation

*correspondence authors: lyuanzou@masdar.ac.ae (Prof. Linda Zou)

This PDF file includes:

1. Experimental videos.

   Video-S1 Real-time hygroscopic process of pure NaCl crystals

   Video-S2 Real-time hygroscopic process of CSNT particles

   Note that these videos were corresponding to Figure 3d, 3e and 3f. in the main manuscript, and were played with a x20 rate from 50 % RH to 75 % RH.
2. Theoretical analysis

   S-I The nucleation theory of water-vapor condensation (Figure S1 and S2)

   S-II Prediction of the critical size as cloud-seeding materials (Figure S3)
3. Experimental section from Figure S4 to Figure S13
4. Instruments for cloud chamber experiments (Figure 14 and S-III)
5. Reference

S-I The theoretical basis of the nucleation of water-vapor condensation

The process of homogeneous nucleation of water-vapor condensation can be regarded as a volume of air supersaturated with water vapor changing to a cloud of droplets.[S1,S2] This can be described thermodynamically in terms of a function called the Gibbs Free Energy (G), which is defined as Equation S1.

$$G = U - TS + PV \qquad \text{(S1)}$$

where U is internal energy, T is absolute temperature, S is entropy, p is pressure, and V is volume. For a uniform system, we can divide by the number of molecules involved, and the result μ is termed the chemical potential. It can be shown that for any closed system at a constant pressure G tends to decrease towards a minimum value, and this provides a means for exploring the development of such systems.

Consider a uniform parcel of humid air with a water vapor pressure p which is greater than the saturated vapor pressure p_0 at the ambient temperature. It can be shown from the definition of G that the chemical potential for a water molecule in the vapor is relative to that in liquid water at the same temperature can refer to Equation S2.

$$\mu_V - \mu_L = kTln(\frac{p}{p_0}) \qquad \text{(S2)}$$

where k is the Boltzmann constant as usual. The free energy increases from the formation of a water droplet of radius r from the vapor according to Equation S3.

$$\Delta G = -\left(\frac{4\pi}{3}\right) r^3 nkTln(\frac{p}{p_0}) + 4\pi r^2 \sigma \qquad \text{(S3)}$$

where n is the number of molecules per unit volume in water and σ is the surface free energy of water per unit area, which is the same as the surface tension for a liquid. When this expression is plotted as a function of radius for the case $P > P_\infty$ corresponding to supersaturated vapor, it has the form shown in Figure S1a with a maximum ΔG^* at radius r^*.

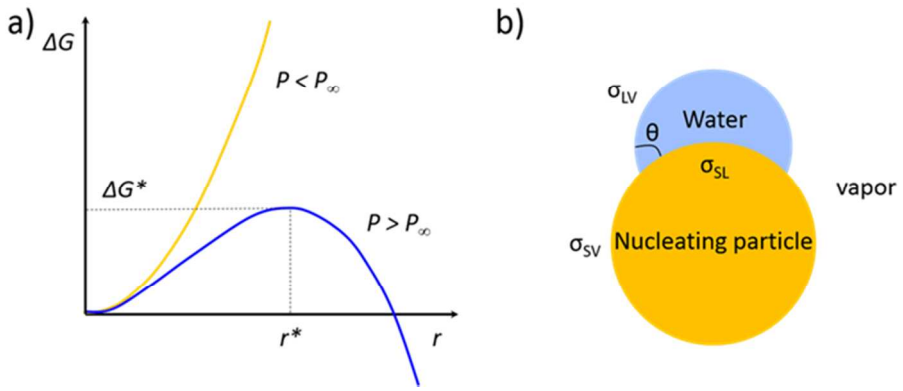

Figure S1. a) The free energy ΔG required to form a liquid droplet of radius r in a vapor with partial pressure p. b) Nucleation of a water droplet on the surface of a solid particle. The contact angle is defined as θ.

In equilibrium, there is a large amount of extremely small droplets in the vapor, and for stable droplet nucleation to occur, it is necessary to surmount the free energy barrier created by this maximum ΔG^*. In order to overcome the free energy barrier, water droplet nucleation requires high degree of supersaturation. For instance, nucleation rate between 10^{-3} and 10^3 droplets per cm^3 /s requires a saturation ratio p/p_0 in the ranger 4.0 to 4.8, which does not exist in atmosphere and can only be achieved in equipment such as cloud chamber.

Accordingly, the case of greatest practical interest is, of course, that of supersaturated vapor. From Figure S1a, we see that for $P > P_\infty$, the free energy involved in the creation of an embryo has a maximum value ΔG^* at a radius r^*. Embryos with radii $r < r^*$ are unstable and tend to

disappear under thermal agitation. On the other hand, embryos with radii $r > r^*$ tend to grow without limit, and become macroscopic droplets. Droplet embryos having the critical radius r* are in unstable equilibrium with the supersaturated vapor.

To find the value of r^*, we set $d\Delta G/dr = 0$, and the Equation-S3 can immediately give to Equation-S4 or S5, which is the Kelvin's classical equations.

$$r^* = \frac{2\sigma}{n_L kT ln(p/p_0)} \qquad \text{(S4)} \quad \text{or}$$

$$\ln(\frac{P}{P_0}) = \frac{2\sigma}{nkTr^*} \qquad \text{(S5)}$$

Solid particles can act as condensation nuclei with a water droplet nucleated on the surface as shown in Figure S1b. As well as the particle radius R, a very important parameter is the contact angle θ of water on the particle surface, defined by the force-balance relation, as seen in Equation S6.

$$\sigma_{SV} = \sigma_{SL} + \sigma_{LV} cos\theta \qquad \text{(S6)}$$

where σ AB is the surface free energy or surface tension between A and B, with S implying the solid particle, L the liquid water, and V the surrounding vapor.

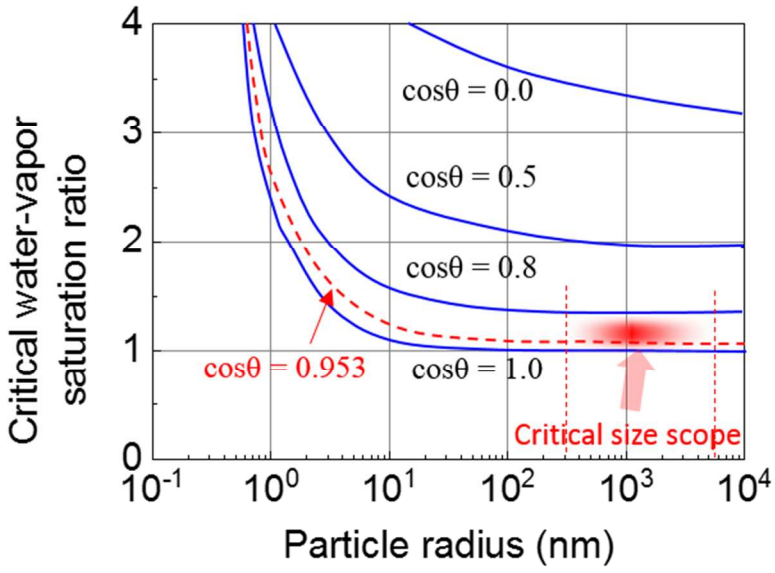

Figure S2. Critical water-vapor saturation ratio and particle size as cloud-seeding materials with different surface properties (θ is the water contact angle of the cloud-seeding materials). Note the contact angle was measured when a water droplet contacted a solid surface of the particle with radius r. The corresponding curve for CSNT-2 can refer to the curve in red color.

With the free-energy barrier ΔG^* being a function of the particle radius r and the contact angle θ, as shown in Figure S2, the nucleation theory can be further extended to underpin the CSNT particle properties. Because the both hydrophobic and smaller particle size require higher supersaturated water vapor pressure, the hydrophobic ultrafine particles do not trigger the rain fall easily.

In addition, since the supersaturation of water vapor pressure in the typical clouds rarely exceeds 1 %, in order to be efficient in rain formation, it is clear that cloud-seeding particles need to have a very small contact angle. Moreover, the optimal size for cloud seeding materials is decided by many factors, such as the condition of the cloud itself (thickness, density and size, *etc.*).

S-II Prediction of the critical size range of CSNT particles as cloud-seeding materials

In general, the above theory can predict the critical size of insoluble particles for water droplet nucleation. As for the CSNT particles, since the surface properties (e.g. contact angle, surface energy) are mainly determined by the TiO_2 shell, it is reasonable to use the above theory to reveal the critical size of the CSNT particles.

As described above, the critical size of cloud-seeding particles is strongly related to its surface hydrophilic performance. Here, we measured the contact angle of CSNT particles (CSNT-2). Note that we used the macro contact angle as an alternative of micro contact angle by preparing the individual particles into a plate with a diameter of 9 mm, as seen in Figure S3. Results showed that the contact angles of CSNT-2 is and 17.6 ° (θ = 17.6 °).

Based on the relationship between critical saturation ratio and the critical particle size of cloud-seeding materials in Figure S2, we can find that the critical size range of CSNT-2 is around 0.4 - 10 μm (please see the curve of cosθ = 0.953), the trend of this curve also indicates that the required critical saturation ratio is not very sensitive to particle size > 0.4 μm when it is very hydrophilic. Thus, this information was used as guidance for the controlling of CSNT particles size during the synthesis. We decided to control the synthesis of the CSNT crystals with the range of 1.4 ± 0.3 μm which fell into the critical size range as mentioned above.

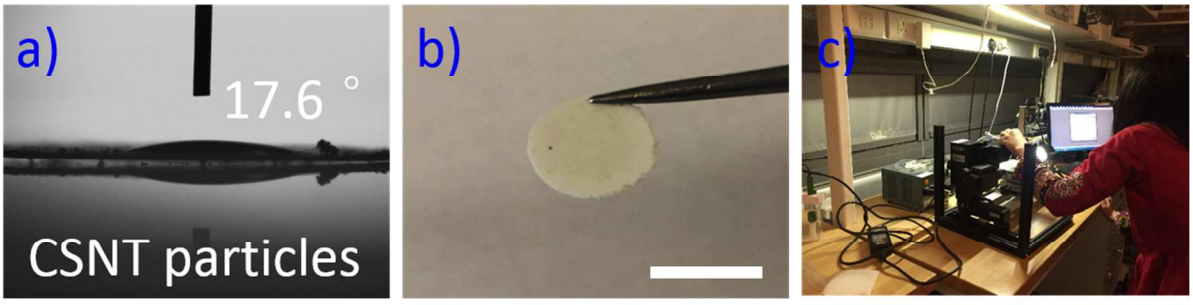

Figure S3. DI water static-contact-angle measurements. Digital images of a) CSNT-2 particles (17.6 °). Note the contact angle value was the 1 s status after contact between water droplet and samples. b) The typical sample (Diameter = 9 mm) prepared by mechanical compression process. The scale bar is 1 cm. c) The water static-contact-angle measurement system (Kyowa DM-701).

Because it is not easy to measure the contact angle of individual microparticle, the plate samples of the corresponding microparticles were prepared through compression molding method. The measured contact angle of plate sample was used as approximation of the one of microparticle.

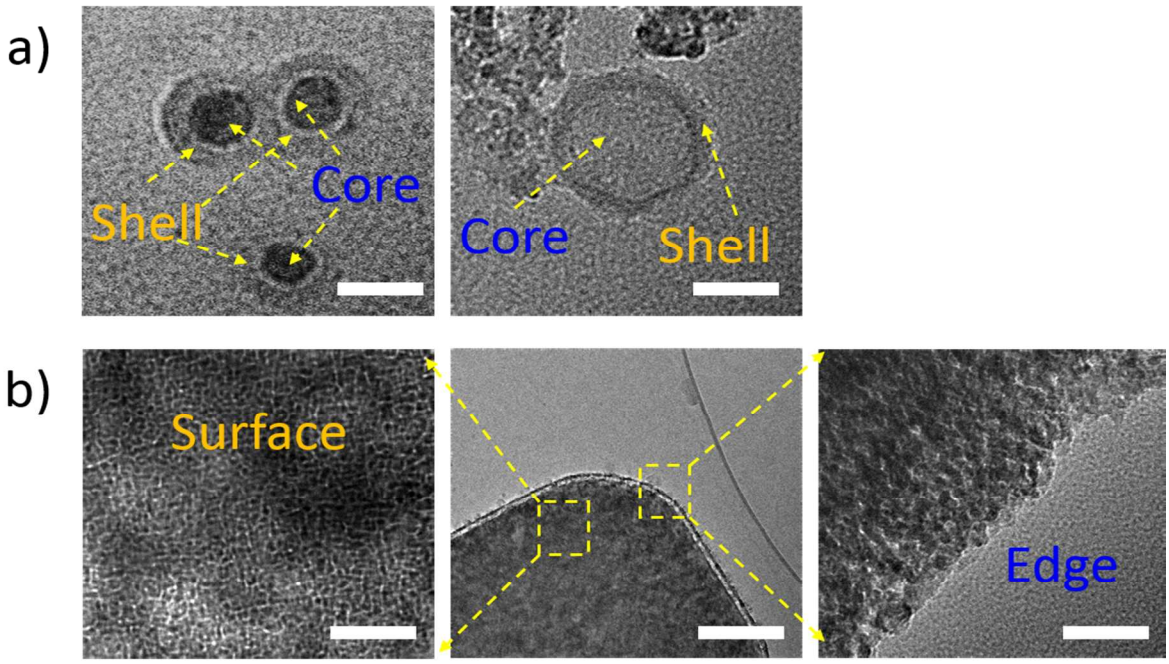

Figure S4. TEM images of a) the synthesized CSNT particles (CSNT-2). The small size further confirmed the feasibility of this synthesis process, Scale bars are 50 nm and 10 nm, respectively. b) Further to show the shell coating of TiO_2 nanoparticles on the surface and the edge of CSNT particles (CSNT-1), scale bars are 10 nm, 50 nm and 10 nm, respectively.

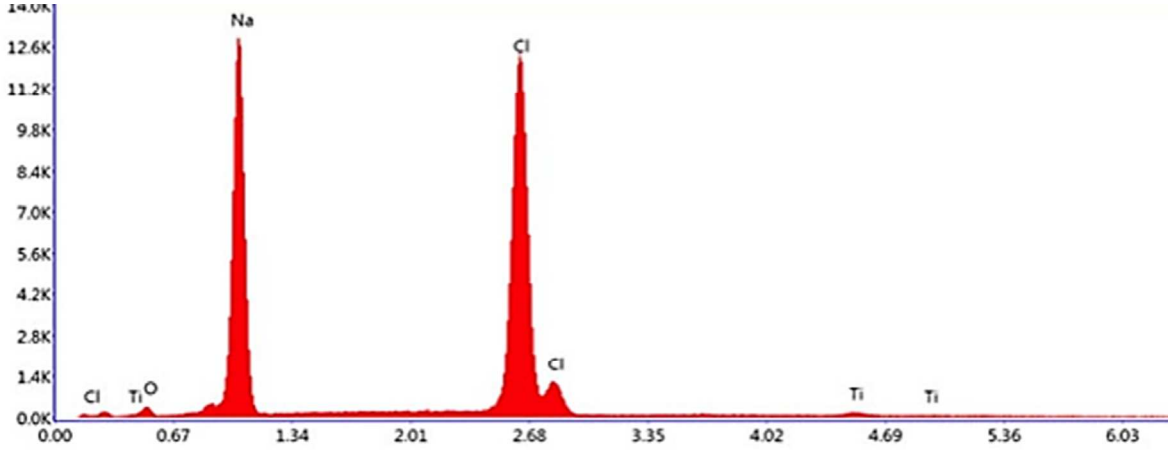

Figure S5. EDX spectrum of CSNT particles (CSNT-2), which is corresponding to Figure 2d in the main manuscript, to further confirm the core/shell microstructure.

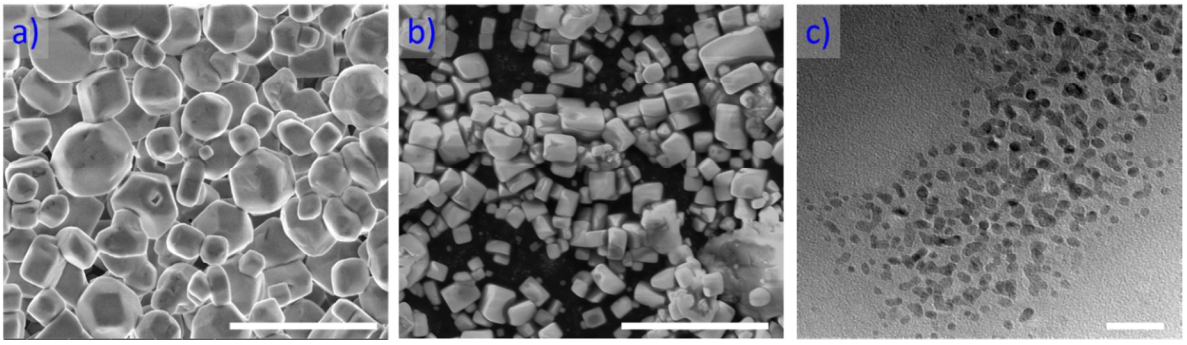

Figure S6. SEM images of the commercial pure NaCl crystals before a) and after b) stone roller process. The scale bars are 10 μm. TEM images of c) TiO_2 particles used for comparison which was synthesized *via* the same process without the loading of NaCl. The scale bar is 10 nm.

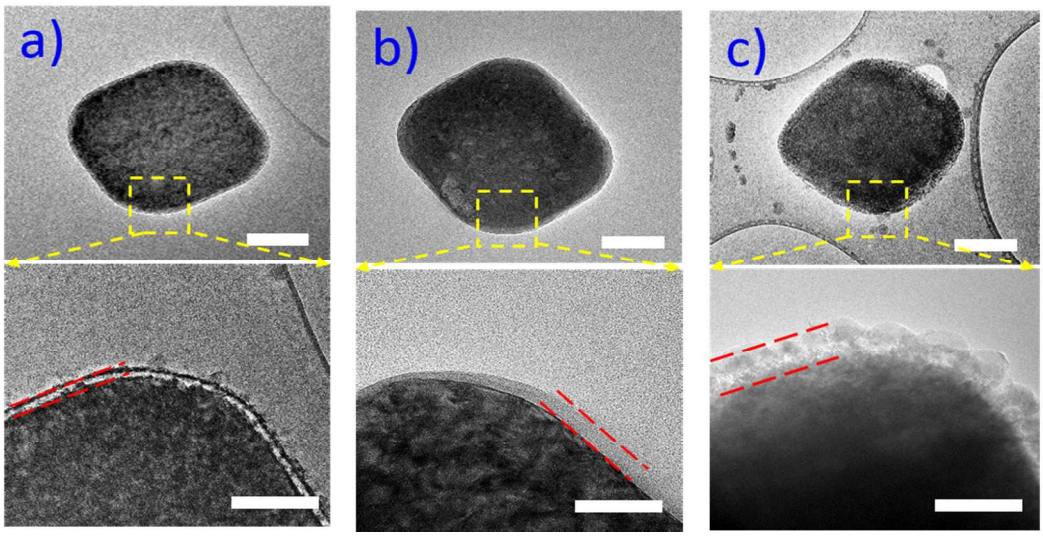

Figure S7. TEM images of CSNT particles with different loading of TiO_2, including 0.196, 0.314, 0.785, respectively, which is the TiO_2/NaCl mixture mass ratios during synthesis process. The scale bar is 200 nm and 50 nm, respectively.

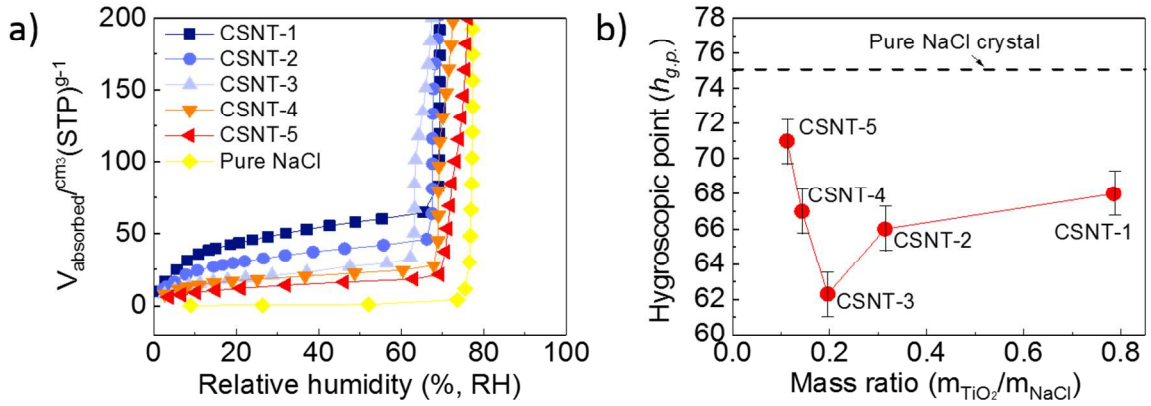

Figure S8. Water-vapor adsorption isotherm tests to reveal the relationship the $h_{g.p.}$ of CSNT particles and the loading of TiO_2 nanoparticles. The mass ratio (m_{TiO2}/m_{NaCl}) is 0.785, 0.314, 0.196, 0.143, and 0.112, the corresponding CSNT particles are defined as CSNT-1, CSNT-2, CSNT-3, CSNT-4, CSNT-5, respectively. All the above data are the average results for three times.

It can be found that when the mass ratio (m_{TiO2}/m_{NaCl}) is 0.196, CSNT particles present a lowest $h_{g.p.}$, ~ 62.5 % RH. As for higher loading of TiO_2 nanoparticles, the shell coating on NaCl crystal is thicker, which is likely to obstruct the diffusion of the adsorbed water-vapor molecules to NaCl core. As for lower loading of TiO_2 nanoparticles, the TiO_2 shell coating is so thin that it could not form an effective moisturizing layer to enable the synergistic effect of forming much larger water droplet at lower vapor-pressure range. This can explain that why the hygroscopic curve of CSNT-5 is close to that of pure NaCl. Other factors such as the water vapor adsorption capacity that contributes to water droplet size also need to be considered apart from the hygroscopic point of the cloud seeding materials, which will be studied in the scale-up application in the future.

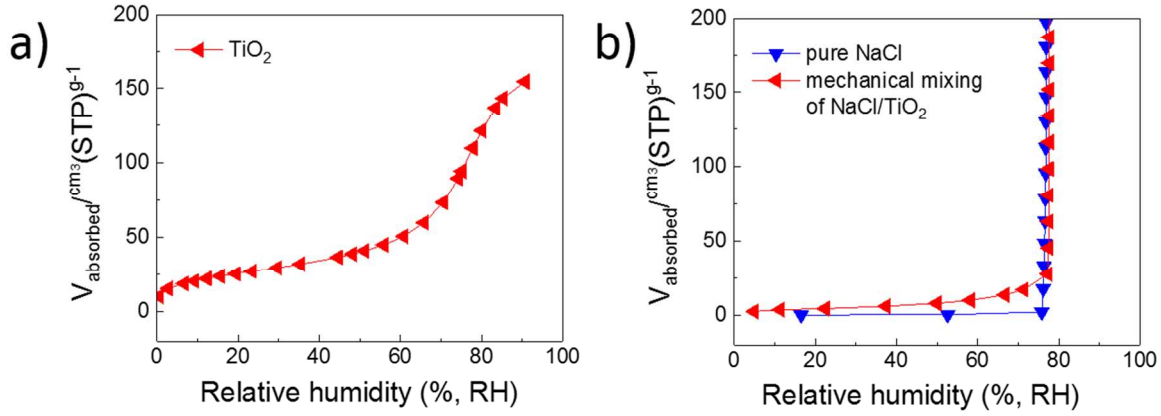

Figure S9. Water-vapor adsorption isotherm tests to characterize the water-vapor adsorption capacity of a) TiO_2 nanoparticle (Diameter = 6 ± 2 nm) and b) the mechanical mixing of NaCl/TiO_2. There is no evident $h_{g.p.}$ for TiO_2 nanoparticle.

It can be found that this enhanced performance of CSNT particles was further confirmed through pure TiO_2 nanoparticles which did not have deliquescent behaviors (*i.e.*, no $h_{g.p.}$), and the mechanical mixing of TiO_2 and NaCl which did not alter the original $h_{g.p.}$ of NaCl.

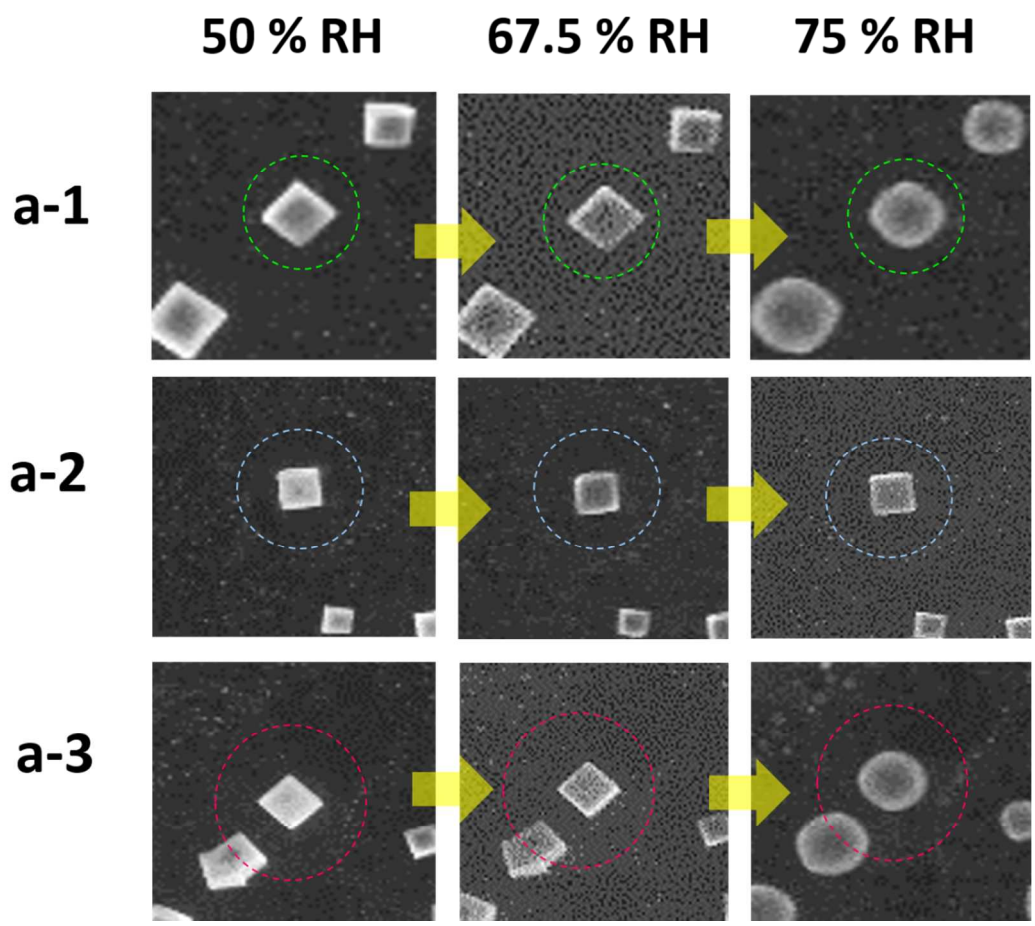

Figure S10. E-SEM images of real-time monitoring the water-droplet growth of pure NaCl as seeding materials at different RH profiles. Note that the images are the magnifications corresponding to the samples (a-1, a-2, and a-3) in Figure 3 (main manuscript).

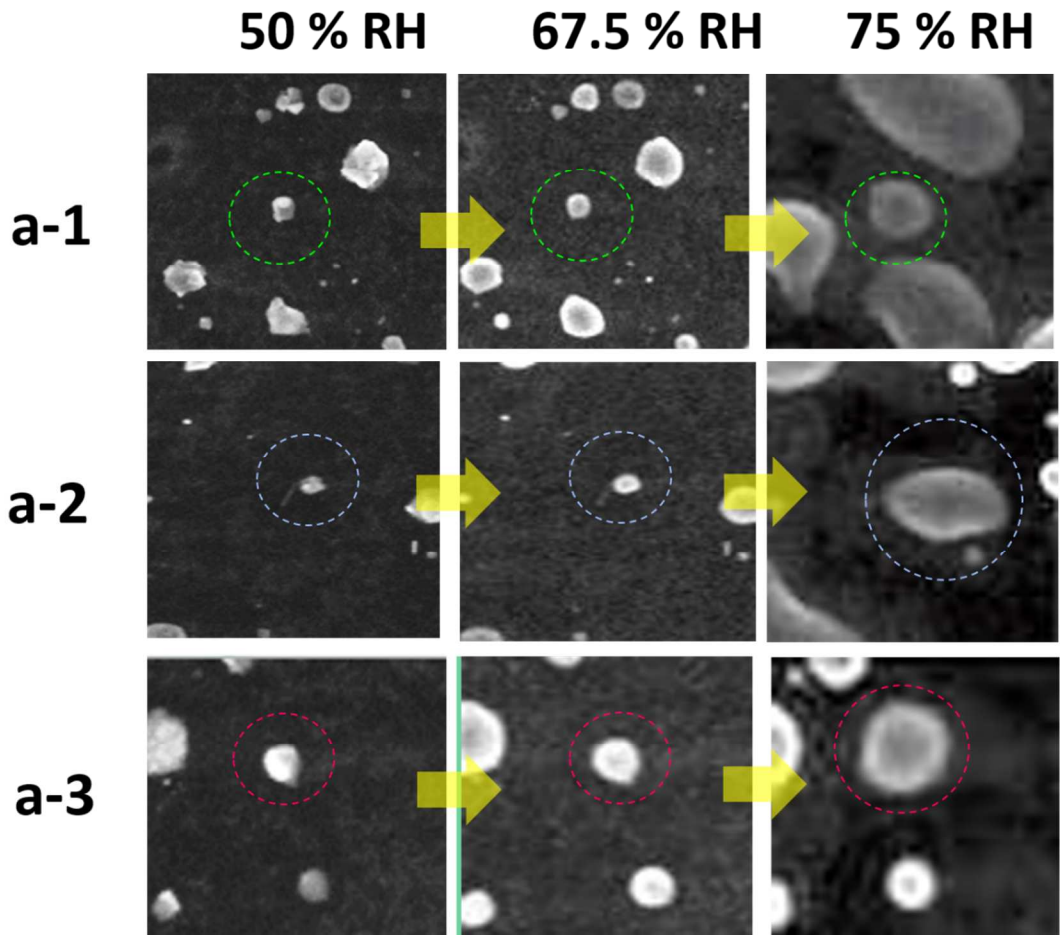

Figure S11. E-SEM images of real-time monitoring the water-droplet growth of CSNT particles as seeding materials at different RH profiles. Note that the images are the magnifications corresponding to the samples (a-1, a-2, and a-3) in Figure 3 (main manuscript).

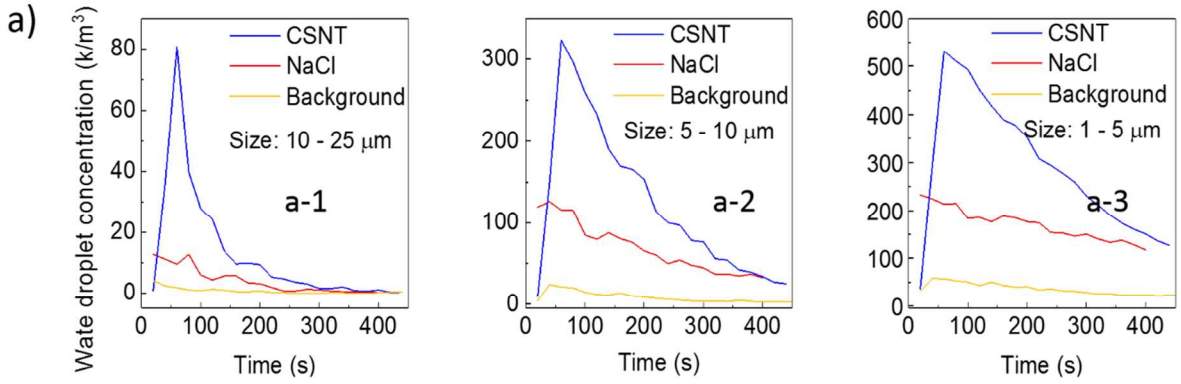

Figure S12. Spectrums of the concentration of water droplets with different sizes: a-1, 10 - 25 μm; a-2, 5 - 10 μm; a-3, 1 - 5 μm; respectively. The chamber conditions were controlled at 5 ℃ and 100 % RH with different cloud-seeding materials as described above. The default loading of NaCl crystals or CSNT particles was 0.05 g for each experiment, and the above data is the average results for three times.

Note that the RH valut of 70 % is very important to verify the efficiency of CSNT particles as cloud-seeding materials, which is above the hygroscopic point (hg.p.) of CSNT particles but below that of pure NaCl crystal.

It can be found that the concentration of water - droplet size between 10 - 25 μm (which is very crucial to the rainfall) caused by CSNT particles was up to 2.9 times higher than that by NaCl, and 39.8 times higher than that of background.

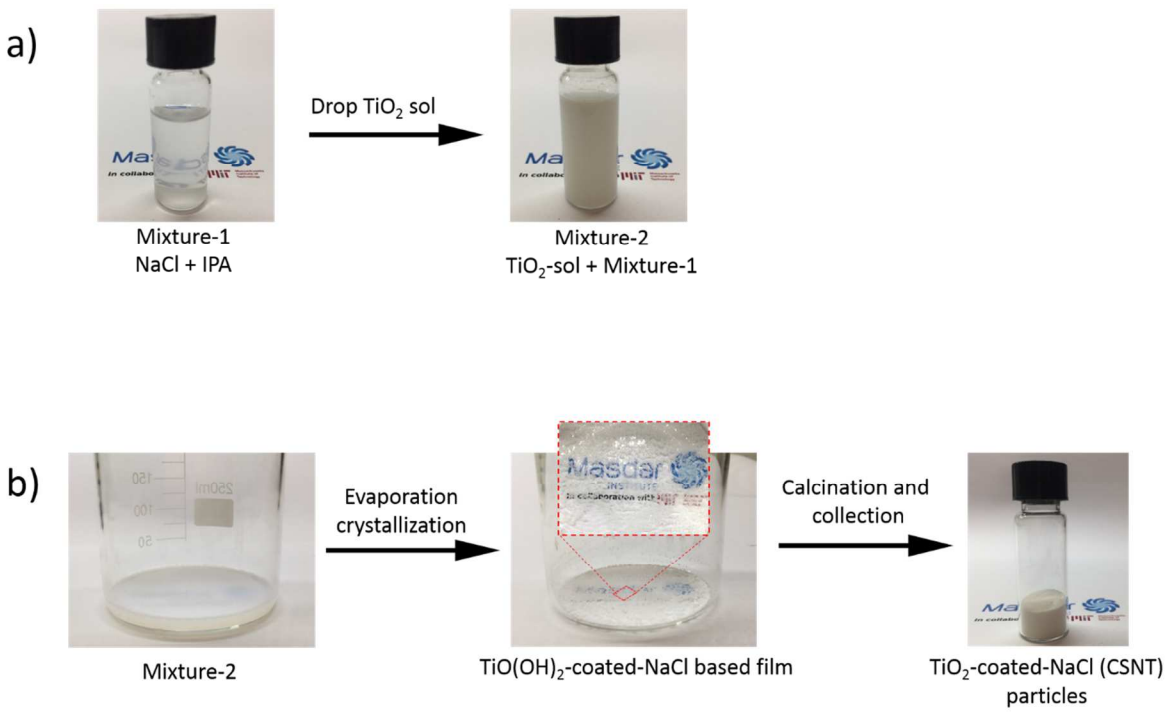

Figure S13. The typical synthesis routes of a) TiO_2 sol and b) CSNT particles.

S-III Instruments for cloud chamber experiments [S3]

--Chamber for laboratory studies of cloudy processes

The cloud chamber (Figure S13a) represents a rectangular container of 8 m^3 with the heat-insulated walls. Inside the camera there is a metal leaf made of galvanized iron and is cooled by means of three refrigerating units. The camera is supplied with temperature adjustment system, and temperature can be maintained in the camera from + 5 °C to + 30 °C. To reduce the temperature gradient, the camera has been pasted over with a special heat-insulating film and four fans for air hashing have been installed. In the camera probes for control of temperature and humidity are placed.

--Aerosols spectrum counter Lasair III 350L

Number concentration of aerosol particles in a chamber was measured by counter Lasair III (Figure S13b). During the experiment the counter was installed in the camera, and data were printed out from the printer which is built in the counter. The aerosol particle counter takes a measurement every 20 seconds from the camera.

--Device for investigation of cloud droplets

For photograph of an area of droplets, MBI-15 microscope with the video camera (Figure S13c) was used.

For capturing of cloud droplets, the drum trap (Figure S13d) was used.

--Device for creation of cloudy environment

For creation of the cloudy environment the device consisting of two humidifiers placed in the plastic container of 100 liters (Figure S13e) has been designed. The device is connected to the camera by means of an aluminum pipe with a diameter of 0.1 m on the container cover, the fan for creation of a stream of damp air is installed in the camera.

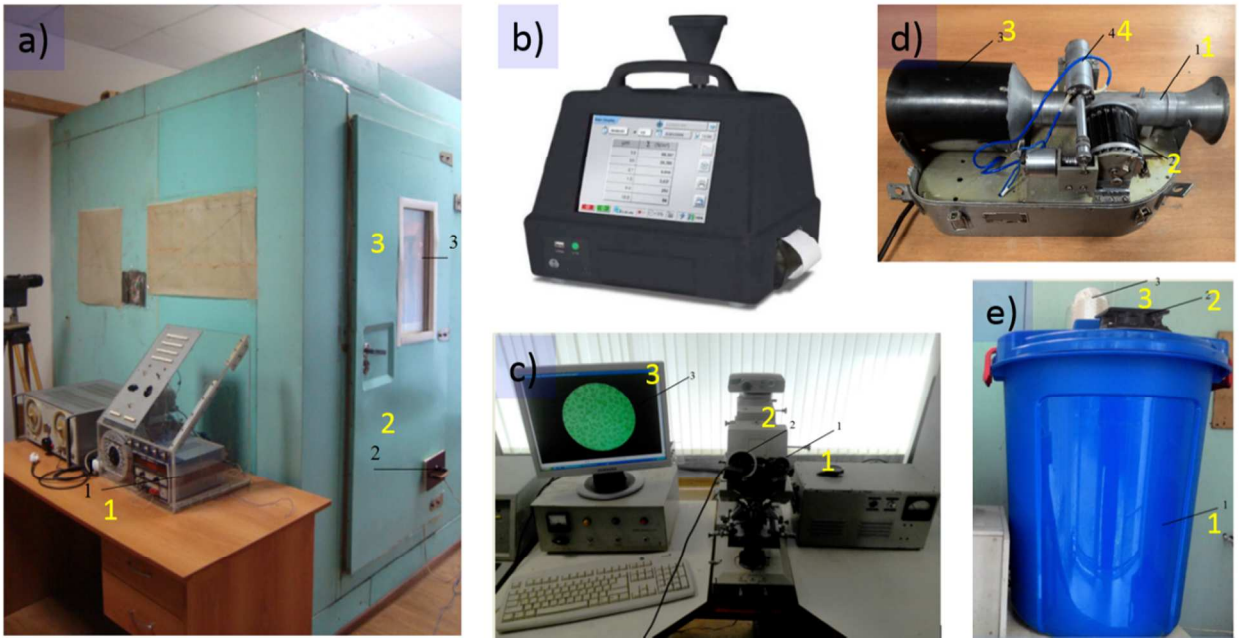

Figure S14. The main instruments used for cloud-chamber experiments. a) Cloud chamber: 1 - control panel; 2 - window for access to the camera during experiments; 3 - observation port. b) Aerosol particles counter Lasair III 350L. c) System for analysis of droplets spectrum: 1 - microscope MBI-15; 2 - video camera; 3 - computer screen. d) Cloud droplets capturing device: 1 - pipe; 2 - drum with glass plates; 3 - fan; 4 - electric motor. e) The device for creation of the cloudy environment: 1 - plastic container; 2 - fan; 3 - aluminum pipe.

Reference

(S1) Fletcher N.H. *The Physics of Rainclouds*. Cambridge University Press. 2011.

(S2) Segal Y.; Khain A.; Pinsky M.; Rosenfeld D. Effects of Hygroscopic Seeding on Raindrop Formation as Seen from Simulations Using a 2000-bin Spectral Cloud Parcel Model. *Atmos. Res*. **2004**, *71*, 3-4.

(S3) O'dowd, C.D.; Aalto, P.; Hmeri, K.; Kulmala, M.; Hoffmann T., Aerosol Formation: Atmospheric Particles from Organic Vapours. *Nature*, **2002**, *416*, 497-504.